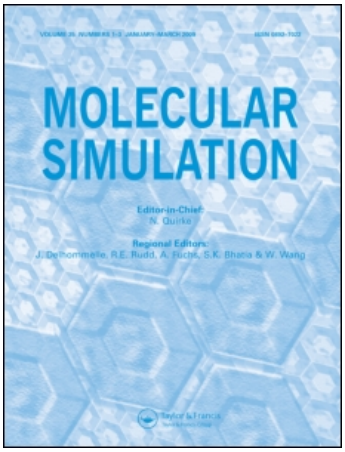

Molecular Simulation
Publication details, including instructions for authors and subscription information:
http://www.informaworld.com/smpp/title~content=t713644482

A Molecular Simulation of A Liquid-crystal Model

Manoj K. Chalam[a]; Keith E. Gubbins[a]; Enrique De Miguel[b]; Luis F. Rull[b]
[a] Cornell School of Chemical Engineering, Univeristy, Ithaca, New York, USA [b] Deaprtmento di Fisica Atomica, Molecular y Nuclear, Universidad de Sevilla, Sevilla, Spain

To cite this Article Chalam, Manoj K. , Gubbins, Keith E. , De Miguel, Enrique and Rull, Luis F.(1991) 'A Molecular Simulation of A Liquid-crystal Model', Molecular Simulation, 7: 5, 357 — 385
To link to this Article: DOI: 10.1080/08927029108022462
URL: http://dx.doi.org/10.1080/08927029108022462

Molecular Simulation, 1991, Vol. 7, pp. 357–385
Reprints available directly from the publisher
Photocopying permitted by license only

A MOLECULAR SIMULATION OF A LIQUID-CRYSTAL MODEL: BULK AND CONFINED FLUID

MANOJ K. CHALAM and KEITH E. GUBBINS[1]

School of Chemical Engineering, Cornell University, Ithaca, New York 14853, USA

ENRIQUE DE MIGUEL and LUIS F. RULL

Departamento di Fisica Atomica, Molecular y Nuclear, Universidad de Sevilla, Aptdo. 1065, Sevilla 41080, Spain

(*Received April 1991, accepted April 1991*)

A Gay–Berne fluid of prolate molecules with length-to-breadth ratio 3 is studied using molecular dynamics simulations. This fluid exhibits vapor, isotropic liquid, nematic, and smectic-B mesophases. For the bulk fluid we report new results along isochores that further delineate the smectic and nematic regions of the phase diagram; the effect of system size is also discussed. These studies lead to a rather complete description of the fluid part of the phase diagram. We have also studied the changes that occur when such a fluid is confined in a pore with parallel, homeotropic walls. Our molecular dynamics results show that the isotropic–nematic transition shifts to higher temperatures, or lower densities, i.e., the liquid crystal phase is stabilized relative to the bulk fluid.

KEY WORDS: Liquid crystal, Gay–Berne fluid, pore

1 INTRODUCTION

In this paper we present the results of a series of NVT molecular dynamics simulations on a system of molecules interacting via the Gay–Berne (G–B) potential model; both the bulk and the confined fluid are studied. Previous simulations [1, 2] and theoretical studies [3] have shown that if these ellipsoidal molecules are long enough (e.g. $\kappa = 3$), the G–B model exhibits isotropic and nematic liquid crystalline phases.

In their computer simulations of hard anisotropic molecules, Frenkel *et al.* [4–10] have shown that hard prolate and oblate ellipsoids of revolution and spherocylinders have a rich phase diagram with nematic, and in some cases smectic and columnar, phases depending on the molecular size and shape. In particular, they argue that hard ellipsoids of revolution are unlikely to form smectic phases. However the Gay–Berne potential, although it possesses an ellipsoidal hard core, can be expected to induce smectic phases because of the stabilizing nature of the anisotropic attractive forces. This is indeed the case from our results described previously [11] and extended here, and from some preliminary simulation results reported by Luckhurst *et al.* using a slightly modified version of the G–B potential [12].

We have previously [13] located the vapor–liquid coexistence curve for the G–B fluid with parameters $\kappa = 3$ and $\kappa' = 5$ using the Gibbs ensemble Monte Carlo simulation method [14]. The coexistence points corresponding to the isotropic–nematic transition

[1]To whom correspondence should be sent.

have also been obtained for two temperatures, $T^* = 0.95$ and 1.25 by calculating the free energy of each phase [2]. For smectic phases it is difficult to devise a thermodynamic integration route, and in this work we therefore adopt an approximate method to locate the phase transitions involving isotropic liquid, nematic, and smectic phases. This method involves the study of the fluid structure, order parameter, heat capacity, and pressure along isochores. These results extend and confirm similar results obtained recently along isotherms [11], and provide a rather complete description of the fluid phase diagram. Using this approximate method, we expect the errors in the coexistence densities and temperatures to be 0.005 and 0.1, respectively. We note that in using this approximate method, the errors in the coexistence densities are not significantly greater than those obtained by the methods of thermodynamic integration.

In addition to these results for the bulk G–B fluid we present a study of the G–B fluid confined between parallel homeotropic walls; the fluid-wall forces tend to orient the molecules normal to the wall. The effect of confinement is to stabilize the nematic phase relative to the bulk fluid.

General considerations of the MD simulations are presented in Section 2. Results for the bulk fluid are presented in Section 3, together with a summary of existing knowledge of the phase diagram for the $\kappa = 3$ G–B fluid, including vapour, isotropic liquid, nematic and smectic phases. The effect of increasing the system size on the isotropic–nematic transition is also examined. In Section 4 we study the G–B fluid confined between parallel plates. Finally, we present our conclusions in Section 5.

2 MOLECULAR DYNAMICS (MD) SIMULATION METHOD

The G–B potential model is [2, 11]

$$u(r, \hat{\mathbf{r}}, \hat{\mathbf{u}}_1, \hat{\mathbf{u}}_2) = 4\varepsilon(\hat{\mathbf{r}}, \hat{\mathbf{u}}_1, \hat{\mathbf{u}}_2)\left[\left(\frac{\sigma_0}{r - \sigma(\hat{\mathbf{r}}, \hat{\mathbf{u}}_1, \hat{\mathbf{u}}_2) + \sigma_0}\right)^{12} - \left(\frac{\sigma_0}{r - \sigma(\hat{\mathbf{r}}, \hat{\mathbf{u}}_1, \hat{\mathbf{u}}_2) + \sigma_0}\right)^{6}\right]$$

where $\hat{\mathbf{u}}_i$ stands for the axial vector of molecule i and $\hat{\mathbf{r}}$ is the unit vector along the intermolecular vector $\mathbf{r} = \mathbf{r}_2 - \mathbf{r}_1$, where $\mathbf{r}_1$ and $\mathbf{r}_2$ are the centres of mass positions of molecules 1 and 2, respectively. Here $\sigma(\hat{\mathbf{r}}, \hat{\mathbf{u}}_1, \hat{\mathbf{u}}_2)$ and $\varepsilon(\hat{\mathbf{r}}, \hat{\mathbf{u}}_1, \hat{\mathbf{u}}_2)$ stand for the range and strength parameters, respectively and are defined explicitly in [15]; σ and ε depend on the anisotropy parameters κ (molecular elongation) and κ' (ratio of the potential well depths of the side-by-side and end-to-end configurations).

The molecular anisotropy and the well depth ratio-parameters in the G–B potential were chosen to be $\kappa = 3$ and $\kappa' = 5$, respectively, as in previous studies. The potential was cut and shifted at $r_c^* = 4$ ($r^* = r/\sigma_0$), and the usual periodic boundary conditions were employed. In all simulations the number of molecules, N, was greater than or equal to 256. The other simulation details are the same as those reported in [2]. The following quantities were monitored during the course of the simulation: pressure (P^*), internal energy per particle (E^*), order parameter $\bar{P}_2$, and structural properties. The director (that is, the direction along which all the molecules align themselves) and the equilibrium second rank orientational order parameter, $\bar{P}_2$, were evaluated by diagonalizing the Q tensor [2, 11, 15]. $\bar{P}_2$ has the values of zero and unity for the isotropic and completely orientationally ordered phases, respectively. The

structural quantities calculated include the orientationally averaged pair distribution function, $g(r)$, second-rank orientational correlation function, $G_2(r) = \langle P_2(\hat{\mathbf{u}}_1, \hat{\mathbf{u}}_2)\rangle$ where $\hat{\mathbf{u}}_i$ is the unit vector along the axis of molecule i, and the orientationally averaged pair correlation functions for two molecules whose centers lie on a line parallel $g_\parallel(r_\parallel)$, or on a line perpendicular $g_\perp(r_\perp)$, to the director. Here the distances $r_\parallel$ and $r_\perp$ are measured parallel and perpendicular to the director, respectively.

The procedure used to start each bulk fluid run was as follows. An f.c.c. lattice was used to generate the initial configuration ($\rho^* = \rho\sigma_0^3 = 0.02$) of N molecules. From low densities, the system was compressed along an isotherm ($T^* = kT/\varepsilon_0$) in a series of steps to the desired density ρ^*. Compression was carried out by decreasing the size of the simulation box, followed by equilibration. At the lower densities (up to about $\rho^* = 0.15$) equilibration was relatively rapid, requiring a few thousand time steps; at the higher densities about 10,000 time steps were needed for equilibration. From these fixed densities, heating/cooling runs were done to determine the various phase

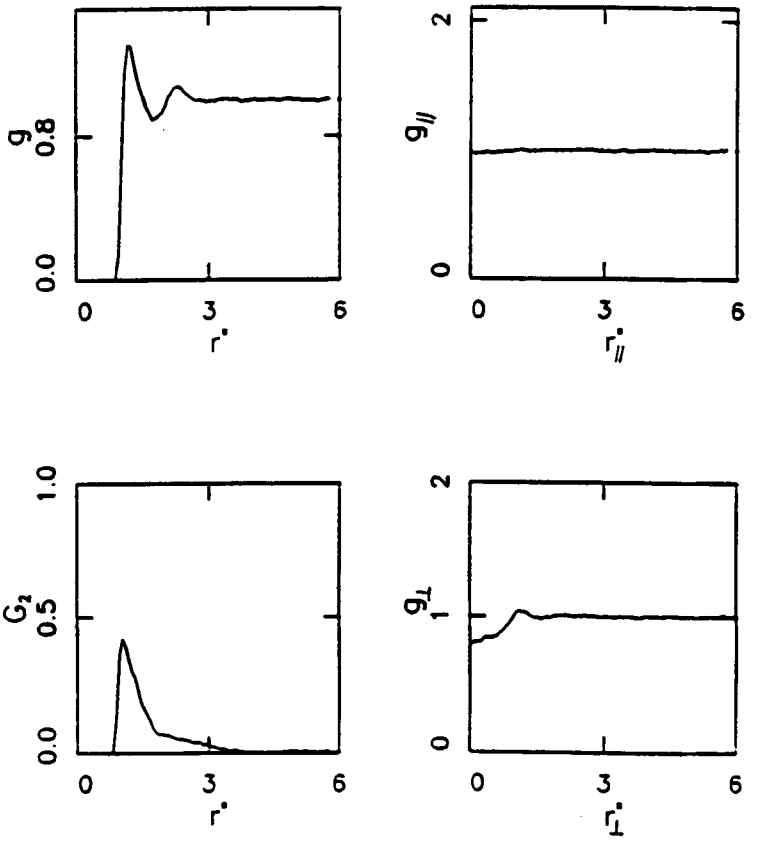

Figure 1 Structure of the isotropic phase at $\rho^* = 0.32$ and $T^* = 1.9$. The figures represent the orientationally averaged pair correlation function $g(r)$, orientation correlation function $G_2(r)$, and the orientationally averaged pair distribution functions that are parallel $g_\parallel(r_\parallel)$ and perpendicular $g_\perp(r_\perp)$ to the director. The distances $r_\parallel$ and $r_\perp$ are measured parallel and perpendicular to the director, respectively.

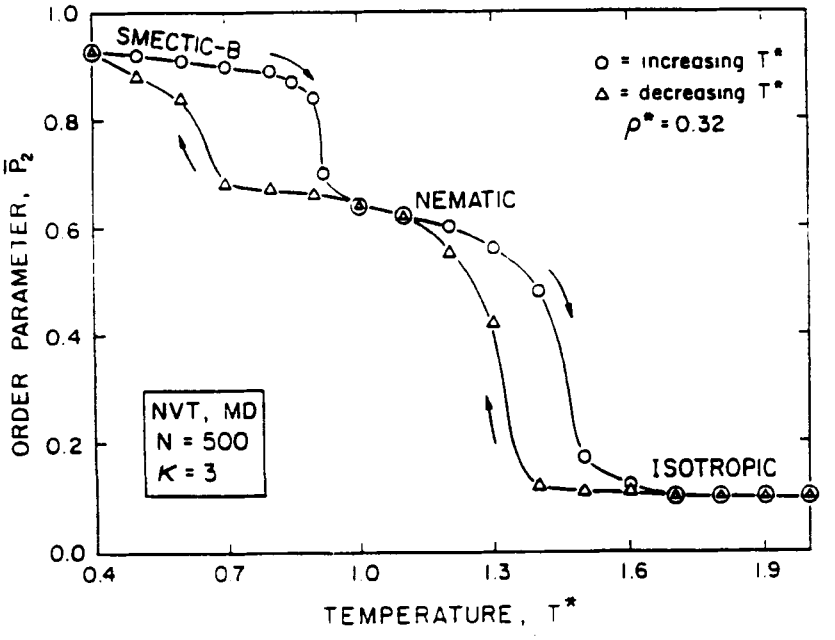

Figure 2 MD results for the order parameter for 500 G–B molecules at $\rho^* = 0.32$; circles are for the heating runs when the system temperature is increased, and squares for the cooling runs.

transitions involved. Table 1 gives details of the simulations, together with the various phases observed.

MD simulations were also performed for the G–B fluid confined between parallel walls using a wall–fluid (w–f) potential $V(z, \theta)$ composed of an isotropic part and an anisotropic part similar to the one proposed by Telo da Gama [16],

$$V(z, \theta) = A\,V(z)\left[1 + \frac{B}{A}\,P_2(\cos\theta)\right] \tag{1}$$

Table 1 Details of the MD simulations for the bulk fluid.

Run	*Type of Run*	*N*	*T**	*ρ**	*Phases Observed*
Isotherms	Compression	256	0.95	0.020–0.370	*I*, *N*, *Sm*
	Expansion	256	0.95	0.290–0.340	*I*, *N*
	Compression	500	0.95	0.020–0.370	*I*, *N*, *Sm*
	Expansion	500	0.95	0.290–0.370	*I*, *N*
	Compression	256	1.80	0.020–0.380	*I*, *N*
	Compression	500	1.80	0.020–0.380	*I*, *N*
	Compression	864	1.80	0.020–0.380	*I*, *N*
Isochores	Cooling	500	0.25–0.65	0.27	*I*, *Sm*
	Cooling	256	0.3–1.9	0.32	*I*, *N*, *Sm*
	Heating	256	0.3–1.9	0.32	*I*, *N*, *Sm*
	Cooling	500	0.3–1.9	0.32	*I*, *N*, *Sm*
	Heating	500	0.3–1.9	0.32	*I*, *N*, *Sm*
	Cooling	500	1.2–5.5	0.38	*I*, *N*, *Sm*

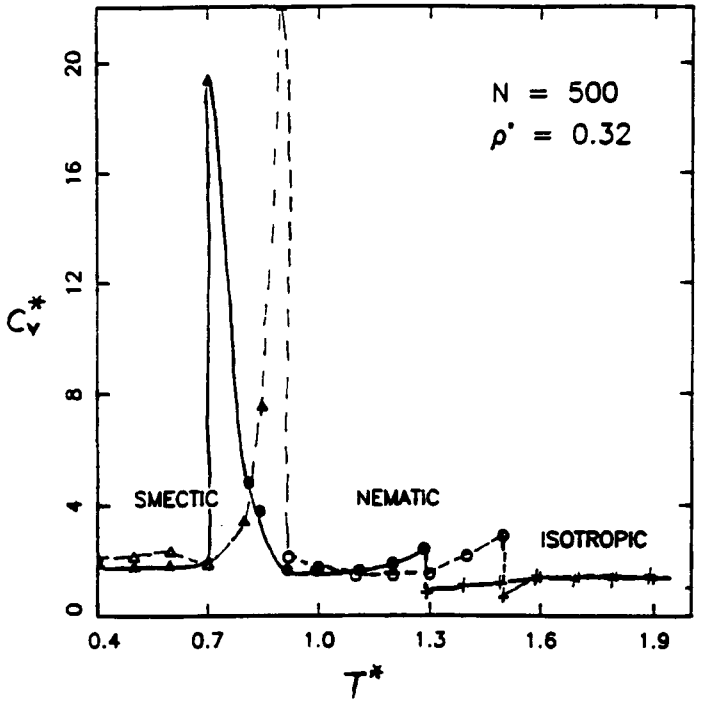

Figure 3 MD results for the heat capacity for 500 G–B molecules at $\rho^* = 0.32$; triangles are for the smectic-B phase, circles for the nematic and pluses for the isotropic. The dashed and solid lines through these points serves as a guide to the eye, and represent heating and cooling runs, respectively.

where A and B are constants that determine the strength of the isotropic and anisotropic parts of the wall-fluid interaction, respectively, and θ is the angle between the molecular axis and the normal to the wall. The isotropic part of the potential $V(z)$, is the (9, 3) wall-fluid potential [17], and at a distance z along the normal to the wall, is given by the following expression

$$V(z) = \varepsilon_w \left[\left(\frac{\sigma_w}{z} \right)^9 - \left(\frac{\sigma_w}{z} \right)^3 \right] \tag{2}$$

with $\sigma_w = 0.71\sigma_0$ and $\varepsilon_w = (10/3)^{1/2}\pi\varepsilon_0\rho_s\sigma_0^3$, where ρ_s is the number density of molecules in the solid wall. When A and B are positive, this potential tends to orient the fluid molecules normal to the wall ($\vartheta = 0$, homeotropic alignment). The basic simulation box is rectangular with the walls in the $z = 0$ and $z = H$ planes, z being the direction normal to the walls. These walls at $z = 0$, H are defined to be the planes where $V(z, \theta)$ becomes infinite. Since the pore walls confine the particles in the z direction, we employ periodic boundary conditions in only the x and y directions. In the simulations, the wall-fluid and the fluid-fluid potentials are of the cut-and-shifted-type with a reduced cutoff distance $r^{*c} = 4\,(r^* = r/\sigma_0)$. Typical equilibration/production runs for 256 and 800 molecules are 20,000/10,000 and 10,000/5,000 timesteps, respectively. The rest of the simulation details are the same as those reported in [2].

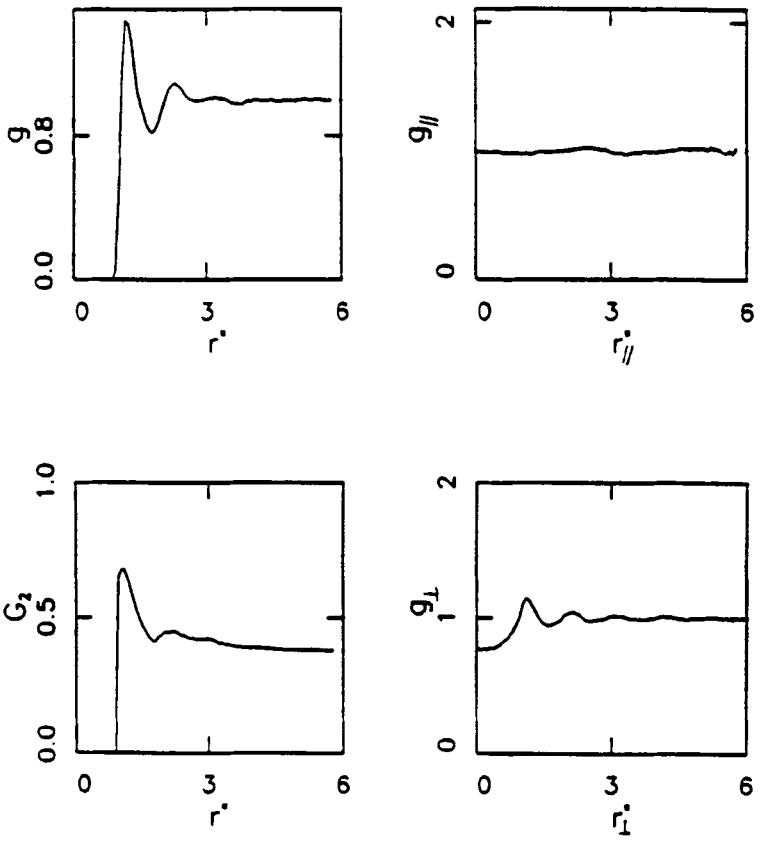

Figure 4 Structure of the nematic phase at $\rho^* = 0.32$ and $T^* = 1.2$.

3 BULK GAY-BERNE FLUID

3.1 Isochores

We first consider the isochore $\rho^* = 0.32$, which exhibits isotropic, nematic and smectic mesophases. At $T^* = 1.9$ the fluid is in an isotropic state with values of $\bar{P}_2 \approx 0.10$; this value is not zero because of the presence of size-dependent short range angular correlations and statistical errors in the evaluation of P_2. In Figure 1 is shown a set of distribution functions which yield information on the structure of an isotropic liquid at this temperature. We see that $g(r)$ is liquid-like and $G_2(r)$ decays to zero at large r, so that there are no long range orientational correlations in the fluid. The other distribution functions, $g_{\parallel}(r_{\parallel})$ and $g_{\perp}(r_{\perp})$, also show no correlations parallel and perpendicular to the director, respectively.

On reducing the temperature along this isochore from $T^* = 1.9$, an orientational disorder–order transition occurs for a T^* somewhat below 1.4; large positive values of the order parameter (Figure 2) indicate an orientational phase change. The heat capacity ($C_v^* = C_v/k_B$), obtained by numerically differentiating the internal energy,

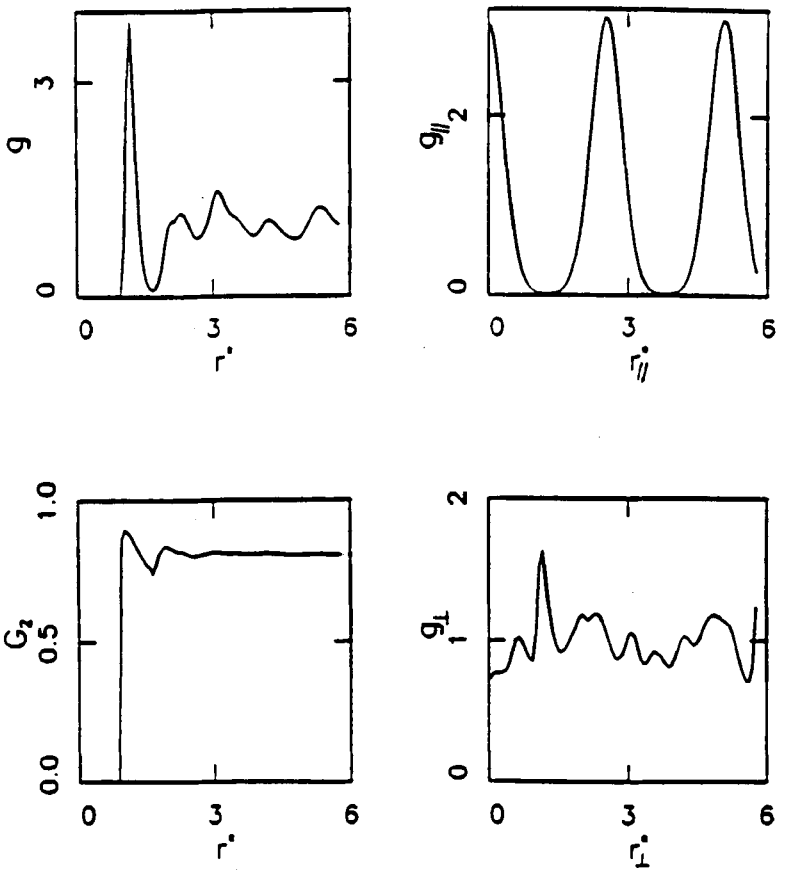

Figure 5 Structure of the smectic-B phase at $\rho^* = 0.32$ and $T^* = 0.7$.

also shows a small peak at $T^* \approx 1.4$ as seen in Figure 3. In Figure 4 the fluid structure is shown at a slightly lower temperature, $T^* = 1.2$. The plot of $G_2(r)$ at large r shows a significant long-ranged orientational order, while $g(r)$ still remains liquid-like, from which we infer that the fluid phase is a nematic. The other distribution functions $g_{\parallel}(r_{\parallel})$ and $g_{\perp}(r_{\perp})$, show no correlations parallel and perpendicular to the director, respectively.

On further reducing the temperature, there is a transition to a new mesophase as seen by a small jump in the order parameter (Figure 2) and a larger peak in the heat capacity (Figure 3). The nature of this mesophase can be understood by plotting the fluid structure as shown in Figure 5. The plot of $G_2(r)$ shows more long-ranged orientational order than the nematic phase while $g(r)$ exhibits some long-ranged translational order. The most significant difference is that the fluid now has a layered structure as seen from the periodic oscillations in $g_{\parallel}(r_{\parallel})$. The spacing between the layers is slightly lower than the molecular length of $3\sigma_0$. The correlations in $g_{\perp}(r_{\perp})$ indicate that the fluid has short-ranged translational order. The layering of the molecules perpendicular to the director is also evident from Figure 6, which shows a snapshot of the centers of mass of the molecules arranged in layers, and with the

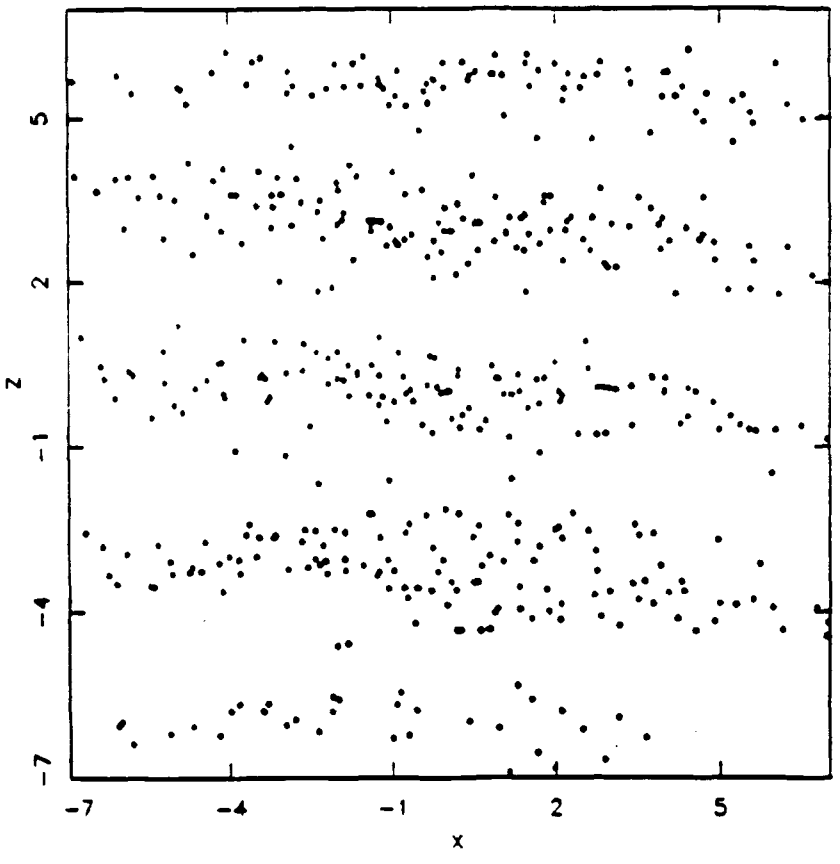

Figure 6 A snapshot showing projections of the molecular centers onto the x–z plane for the final configuration at $\rho^* = 0.32$ and $T^* = 0.7$. The director of the liquid crystal is along the z-direction.

director in the z-direction being orthogonal to the layers. In Figure 7 is shown a plot of the center of masses of the molecules within a layer, i.e., the cross-section of the molecules lying in the x–y plane. The molecules in the layer have a roughly hexagonal arrangement, so we identify the structure to be that of a hexagonal smectic-B phase. Snapshots of the cross-sections of different layers show that there appears to be some short range correlations between the molecules in different layers, but it is difficult to conclusively state from a *NVT* simulation with this system size whether the correlations are short ranged as in a smectic-B phase or long ranged as in a crystal-B phase [18]. The same difficulty in distinguishing between smectic-B and crystal-B phases was reported by Luckhurst *et al.* [12] in their *NVT* simulations of 256 molecules interacting with a modified G–B potential. Both the *I–N* and the *N–SmB* transitions exhibit hysteresis in the transition region, as has been reported in simulations of other first order systems [19]. Snapshots of the final molecular configurations for several temperatures along the $\rho^* = 0.32$ isochore are shown in Figure 8, and display typical isotropic, nematic and smectic-B phases.

For the low density isochore $\rho^* = 0.27$ the fluid undergoes an isotropic to smectic-B transition without forming an intermediate nematic phase. In Figure 9 the order

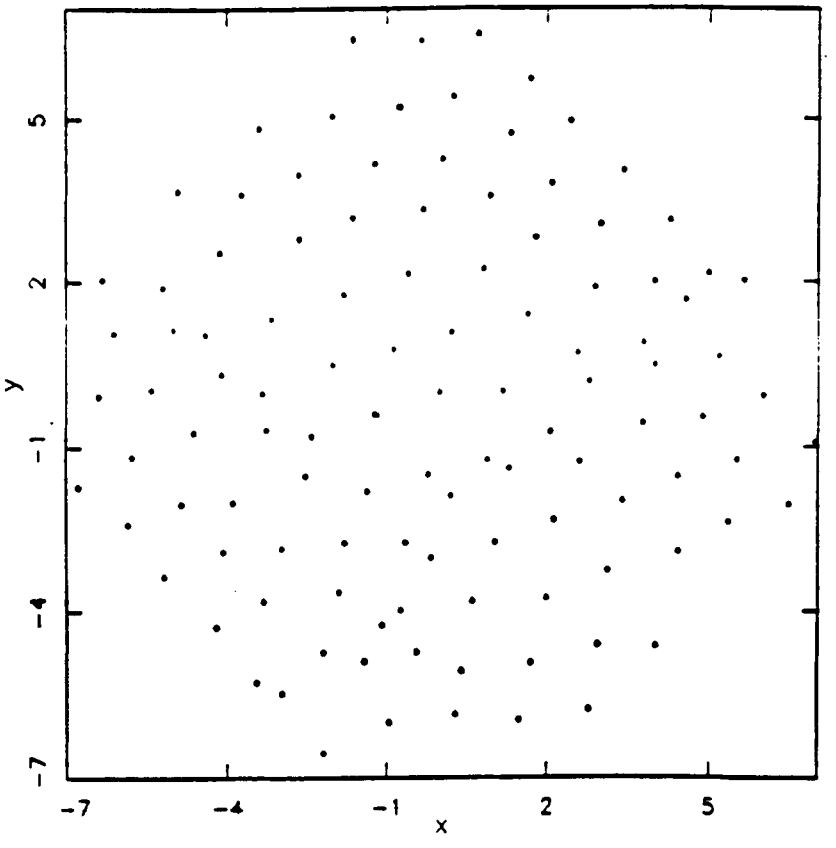

Figure 7 A snapshot of the center of masses of the molecules of the central layer of Figure 6; the cross-section of the molecules lies in the x–y plane.

parameter is displayed as a function of temperature along this isochore. At higher temperatures ($T^* \geqslant 0.60$), $\bar{P}_2$ values are approximately zero, corresponding to an isotropic liquid phase. At lower temperatures ($T^* \leqslant 0.55$), large positive values of $\bar{P}_2$ indicate an orientationally ordered phase. The phase transition is also indicated by a large peak in the heat capacity plot at $T^* = 0.57$, shown in Figure 10. The nature of the orientationally ordered phase can be deduced from plots of the fluid structure; an example is shown for $T^* = 0.55$ in Figure 11. The periodic oscillations in $g_{\parallel}(r_{\parallel})$ and the short-range correlations in $g_{\perp}(r_{\perp})$ indicate a smectic-B-like phase. This is also corroborated from the snapshots of the fluid molecules in the cross-sections in each layer, which are similar to those in Figure 7.

A summary of the approximate transition temperatures of the various mesophases obtained from isochores results is shown in Table 2. The transition temperatures are estimated from the peaks in the heat capacity plots from the cooling runs (see Figures 3 and 10).

3.2 Effect of System Size

As a test of the system-size effect on the I–N transition, we performed several runs at a higher temperature ($T^* = 1.80$) using $N = 256$, 500 and 864 molecules. The

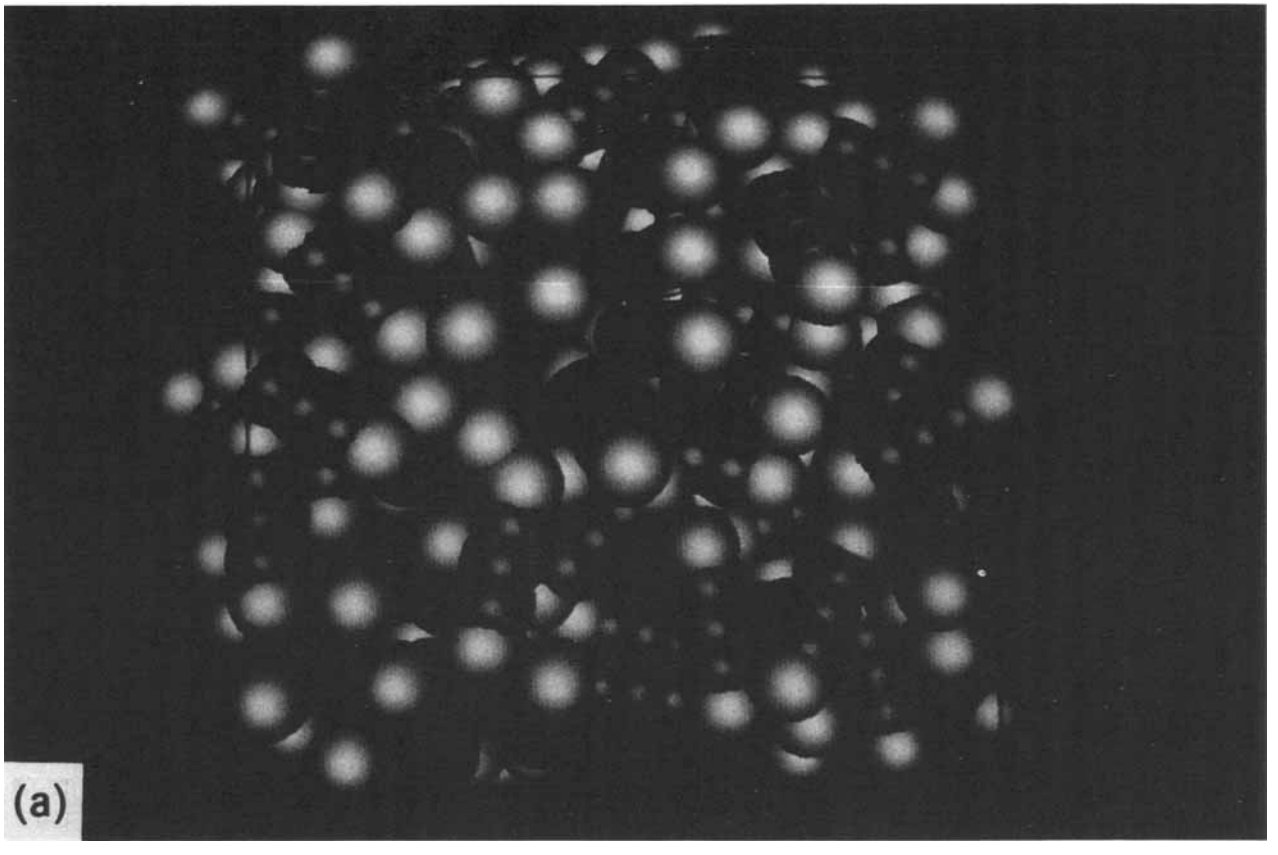

Figure 8 Snapshots of the final configurations obtained from the MD simulations along the isochore $\rho^* = 0.32$. The G–B molecule is represented as a spherocylinder made up of 5 overlapping spheres; the middle 3 spheres are coloured green and the end spheres, red. The figures are at the following temperatures: (a) $T^* = 1.9$; (b) $T^* = 1.2$; (c) $T^* = 1.2$ with the molecular sizes reduced to 25% for better visibility, (d) $T^* = 0.7$ with molecular sizes reduced to 25% (See color plates II–V).

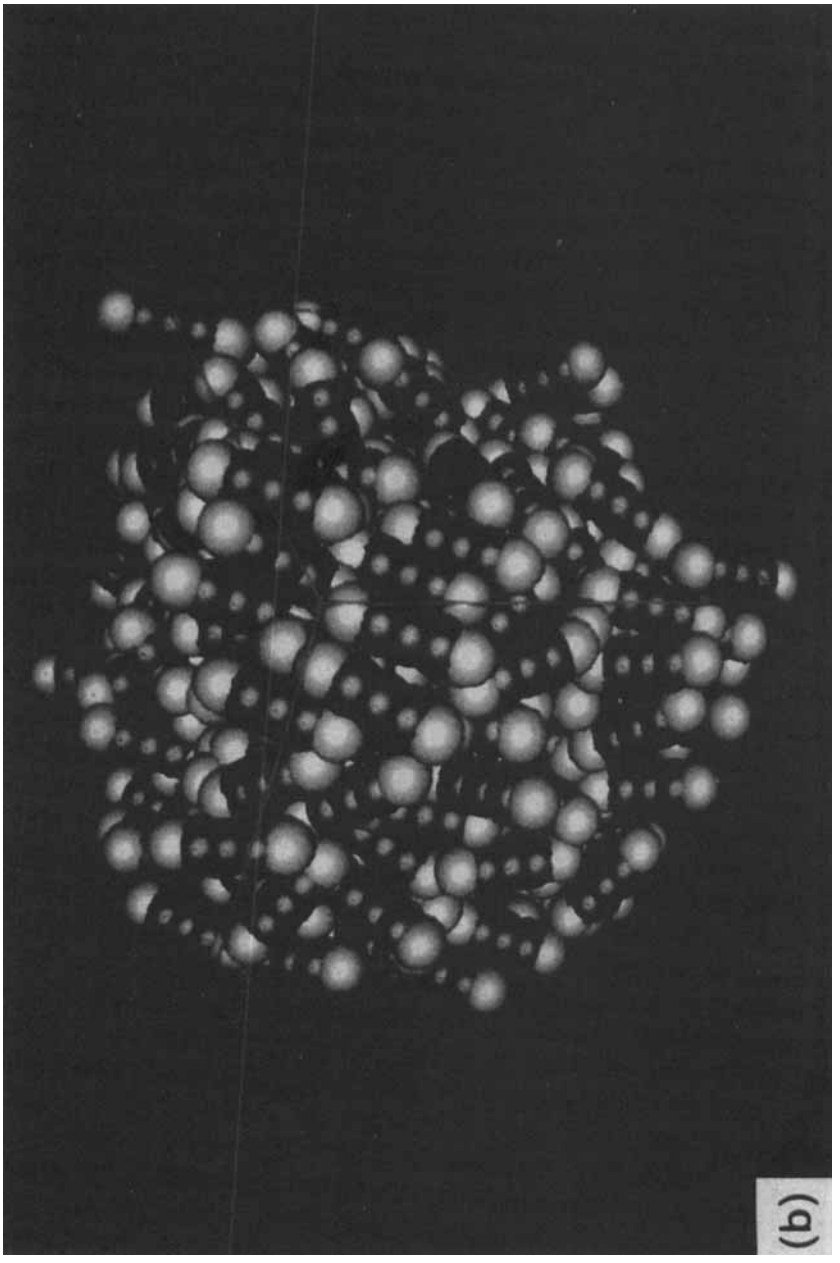

Figure 8 (*Continued*)

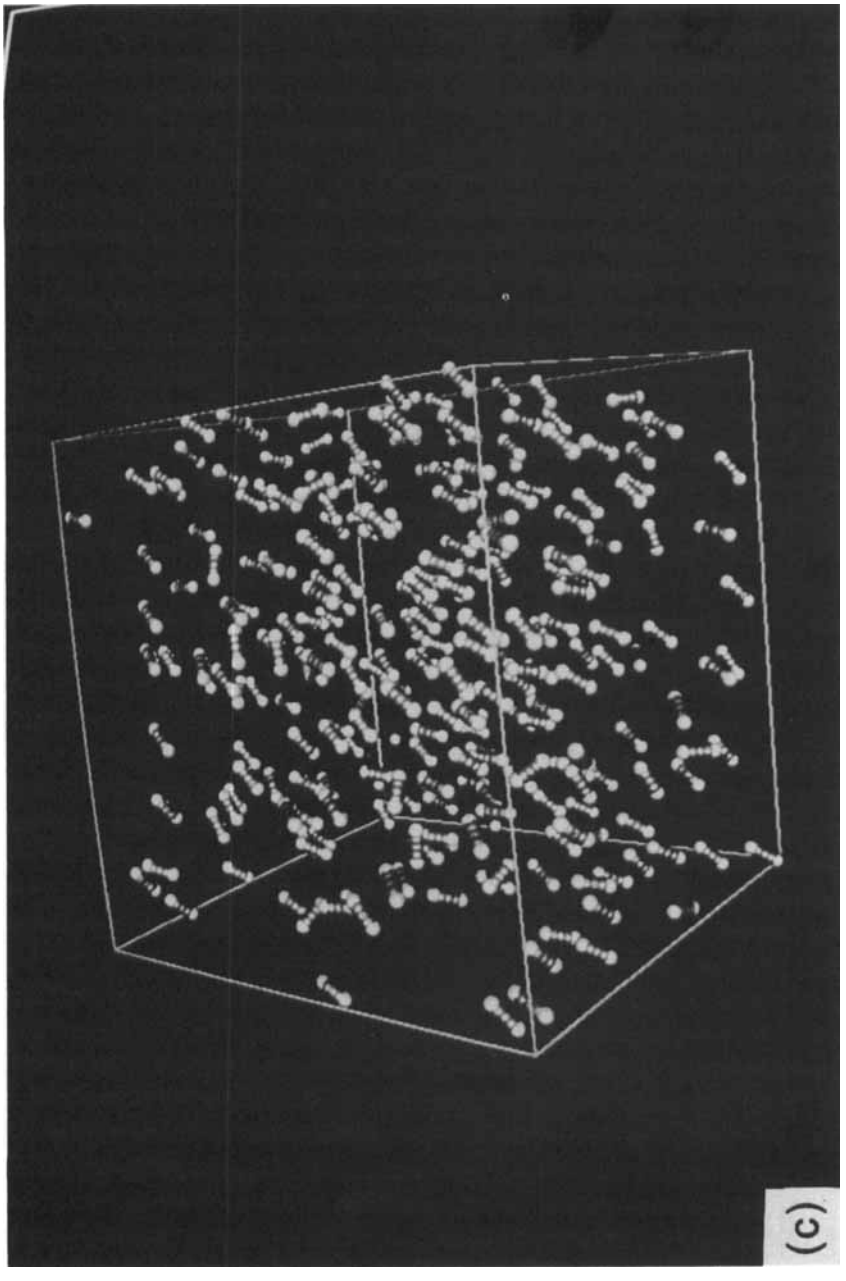

Figure 8 (*Continued*)

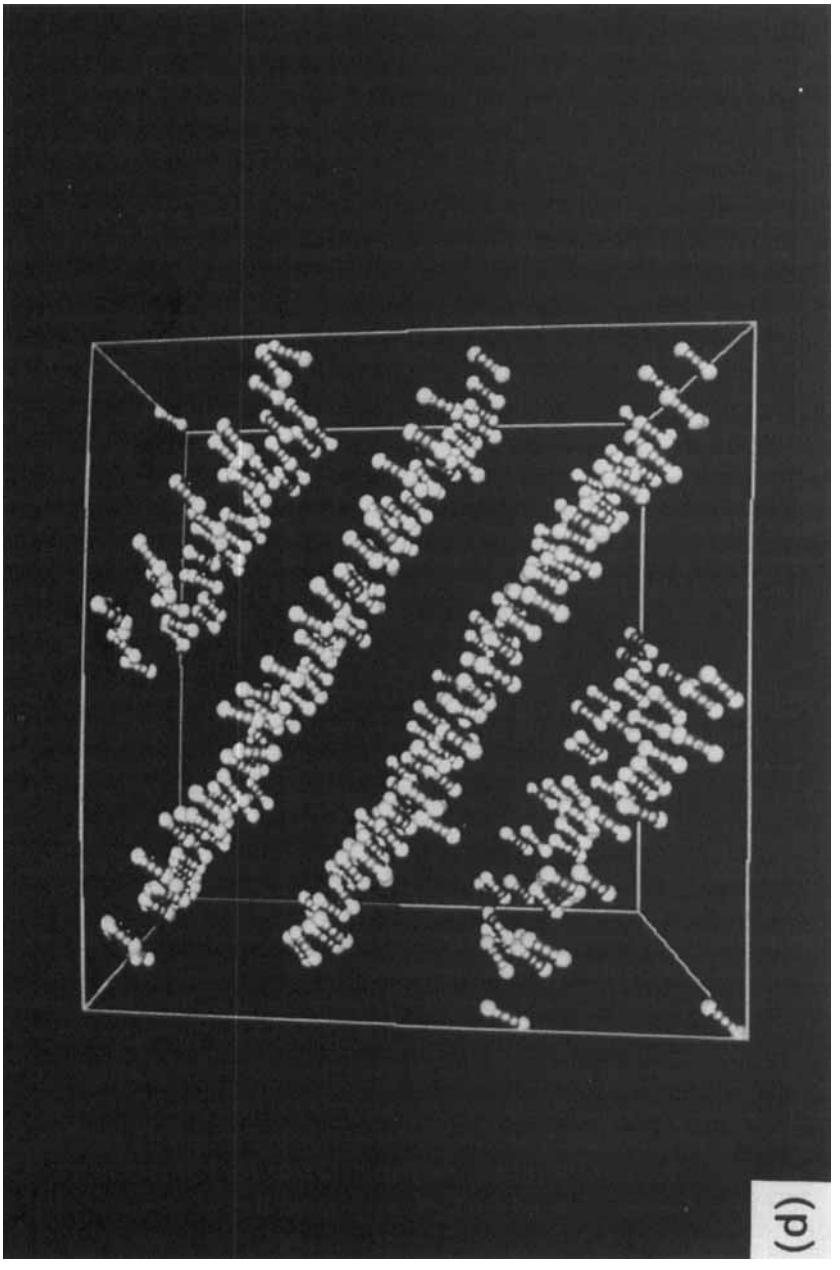

Figure 8 (*Continued*)

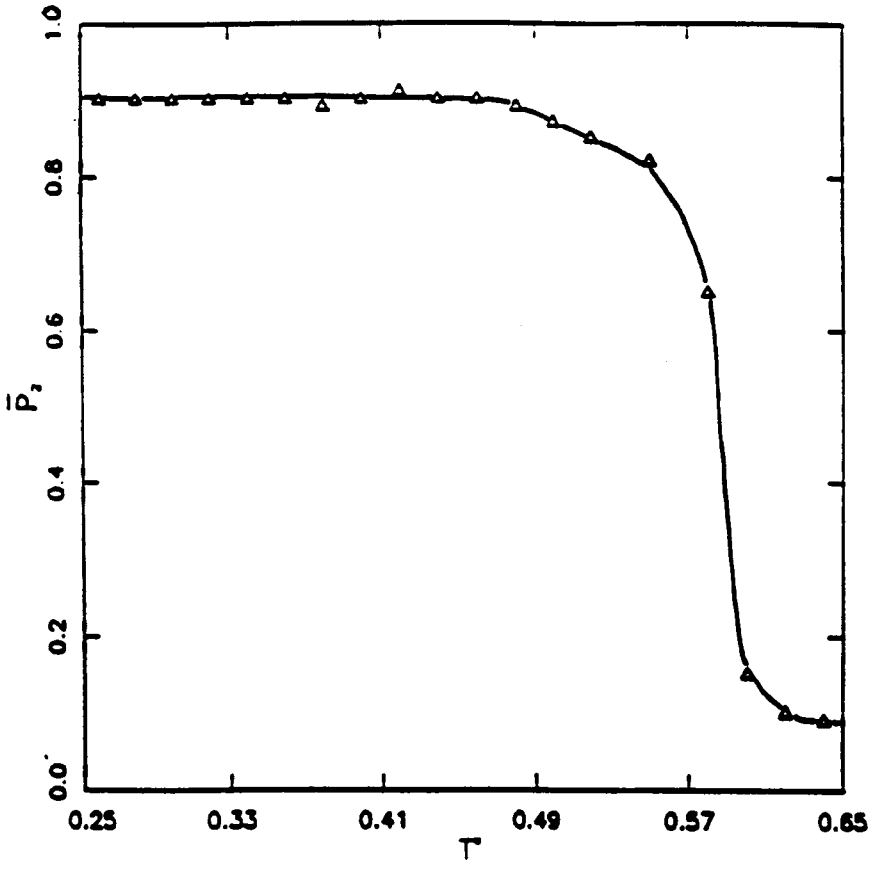

Figure 9 MD results for the order parameter for 500 G–B molecules along the isochore $\rho^* = 0.27$ (cooling).

pressure versus density results are shown in Figure 12 at $T^* = 1.8$. No appreciable system size dependence was found in the equation of state results in the isotropic and nematic regions but the transition region seems to be somewhat affected by the system size. We show in Figures 13 and 14 simulation results for the pressure and configurational internal energy per particle close to the *I–N* transition region. Even though we did not calculate the exact location of the transition densities, these results show that there is a slight shift in the transition densities and pressures as N increases; this shift in density and pressure is very small for N values of 256 and above. An examination

Table 2 Bulk fluid isochores: approximate equilibrium temperatures at the *I–N*, *N–SmB* and *I–SmB* transitions for a system of Gay–Berne molecules with $\kappa = 3$.

ρ^*	$T^*_{I\text{-}N}$	$T^*_{N\text{-}SmB}$	$T^*_{I\text{-}SmB}$
0.27	–	–	0.57
0.32	1.2	0.8	–
0.38	5.2	1.8	–

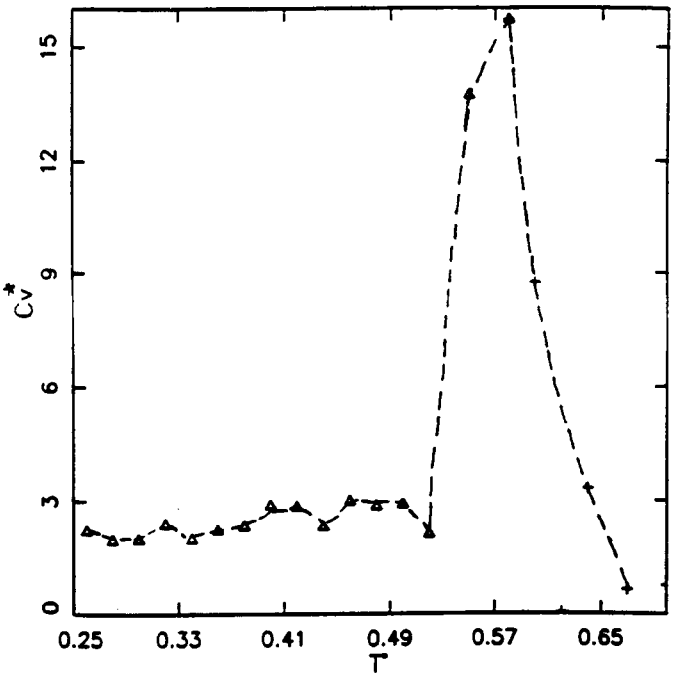

Figure 10 MD results for the heat capacity for 500 G–B molecules at $\rho^* = 0.27$; triangles are for the smectic-B and pluses for the isotropic phase. The dashed line through these points serves as a guide to the eye.

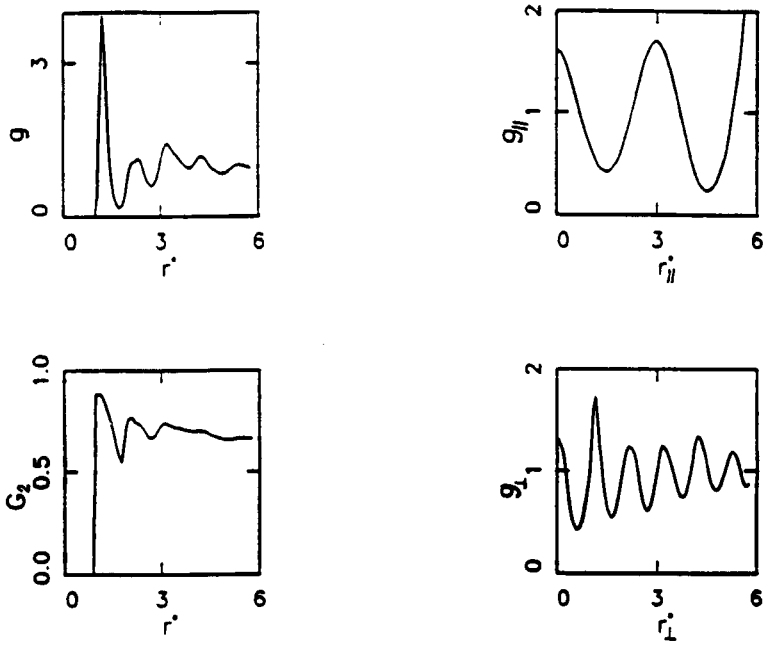

Figure 11 Structure of the smectic-B phase at $\rho^* = 0.27$ and $T^* = 0.55$.

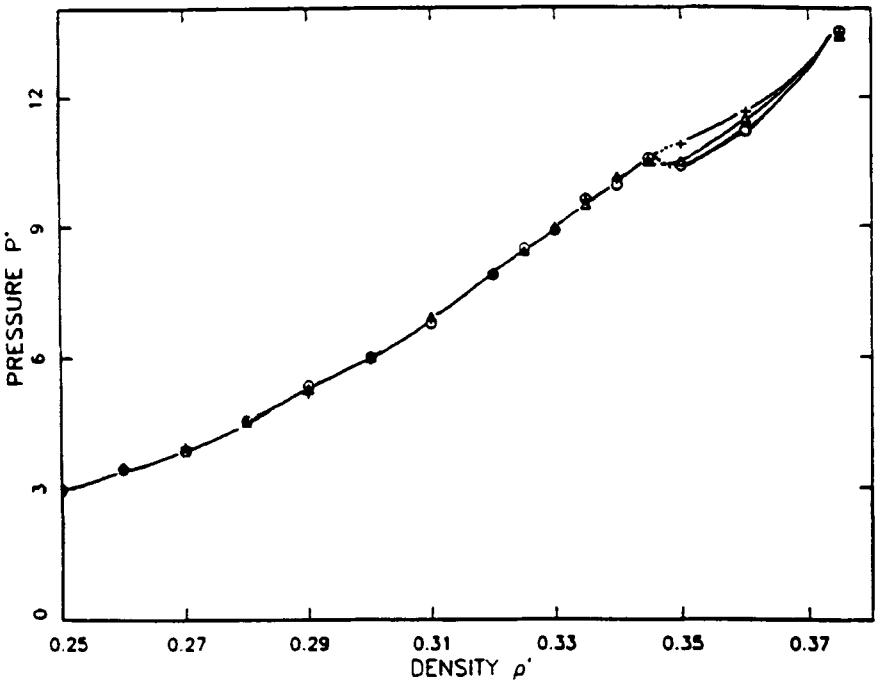

Figure 12 MD results at $T^* = 1.8$ for the equation of state for the G–B system at different systems sizes; circles are for $N = 256$, triangles for $N = 500$, and pluses for $N = 864$.

of structural properties showed that the system was clearly isotropic at $\rho^* = 0.340$ and nematic at $\rho^* = 0.350$. The discontinuity in the internal energy at the transition becomes smoother with increasing N, showing that the I–N transition becomes more weakly first order as N increases. This can also be inferred from the pressure versus density plot, where the metastable region (dashed lines in Figures 13 and 14) becomes wider for the lowest system size. We did not observe any systematic dependence of the isotropic phase results on N. From the results in Figures 13 and 14, we infer that the coexistence pressure P^* is about 10.2, and the coexisting densities ρ^* are close to 0.340 and 0.350 for the isotropic and nematic phases, respectively, at $T^* = 1.8$.

Hysteresis effects are observed in the I–N transition and pre-transition region, though these effects are reduced for larger N values, as seen in Figures 13 and 14. In the transition and pre-transition regions, somewhat different $P^* - \rho^*$ relations are found when the density is successively increased as opposed to decreased. On increasing the density of the isotropic liquid, we found that only a slight compression of this phase past the true transition density was possible before the transition to a nematic phase took place. On the other hand, on starting with a dense nematic phase, it was possible to expand this phase considerably past the transition point before the transition to the isotropic liquid took place. The results at $T^* = 1.8$ shown in Figures 13 and 14 were obtained by successively increasing the density.

We have also studied hysteresis effects for the I–N and *SmB* transitions along the isotherm $T^* = 0.95$ using systems with 256 and 500 molecules (see Figure 15). Coexistence densities for T^* values of 0.95 and 1.80 are shown in Table 3. It should

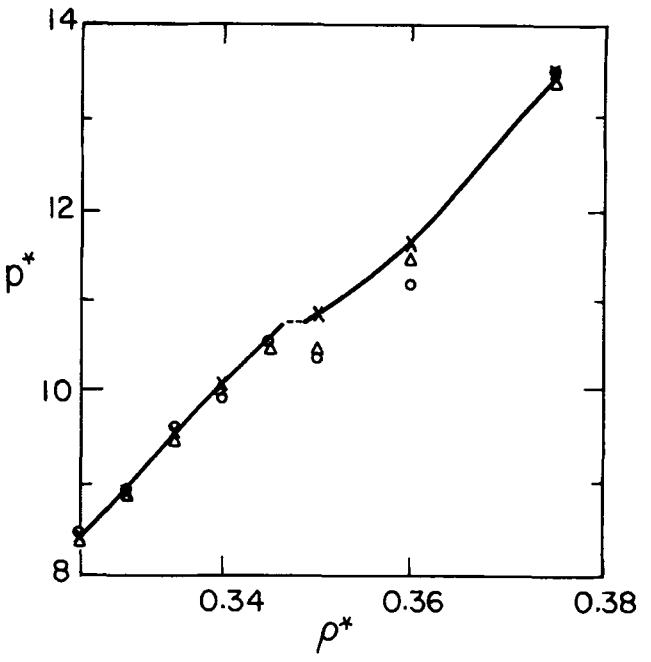

Figure 13 System-size dependence of the pressure in the *I–N* transition at $T^* = 1.80$ for 256 (circles), 500 (triangles), and 864 (crosses) G–B molecules. The solid lines are drawn through the points, and are meant as a guide to the eye; the dashed line approximately locates the transition.

Table 3 Bulk fluid isotherms: approximate coexistence densities at the *I–N*, *N–Sm*B and *I–Sm*B transitions for a system of Gay–Berne molecules with $\kappa = 3$.

T^*	ρ_I^*	ρ_N^*	ρ_N^*	ρ_{SmB}^*
0.95	0.308	0.314	0.345	0.350
1.8	0.340	0.350	–	–

be noted that we did not find a smectic phase upon compression of the nematic phase at $T^* = 1.8$. We believe that the system was trapped in a metastable region which prevents the onset of the smectic phase. However, simulation along the isochore $\rho^* = 0.38$ does show a stable smectic phase at $T^* = 1.8$ (see Table 2).

3.3 Phase Diagram

Based on the coexistence densities reported here (Tables 2 and 3) together with those from previous work [2, 11, 13], we can construct an approximate phase diagram for the $\kappa = 3$ G–B fluid, identifying the vapor, isotropic liquid, nematic and smectic-B phases. This is shown in Figures 16 and 17 for the low and high temperature regions, respectively. The Gibbs ensemble simulations used for the vapor–liquid region [13] indicated the existence of a vapor-isotropic-smectic-B triple point at $T^* \approx 0.4$, and a vapor-isotropic liquid critical point at $T^* = 0.49$ and $\rho^* = 0.096$. From the simulation results in the high density region, we also identify an isotropic-nematic-smectic-B triple point at $T^* \approx 0.8$. Previous results along isotherms using the methods

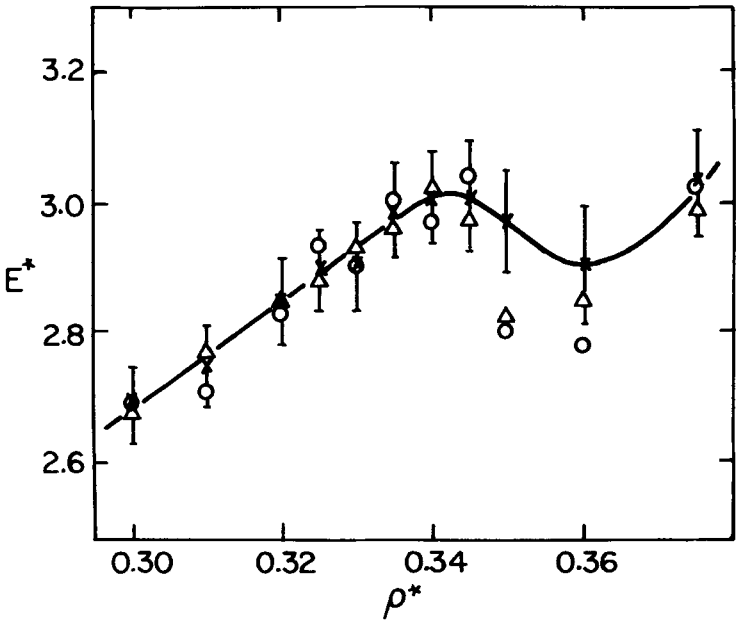

Figure 14 The same as in Figure 13, but for the total energy per particle. The solid line is drawn through the points for the 864 molecule system.

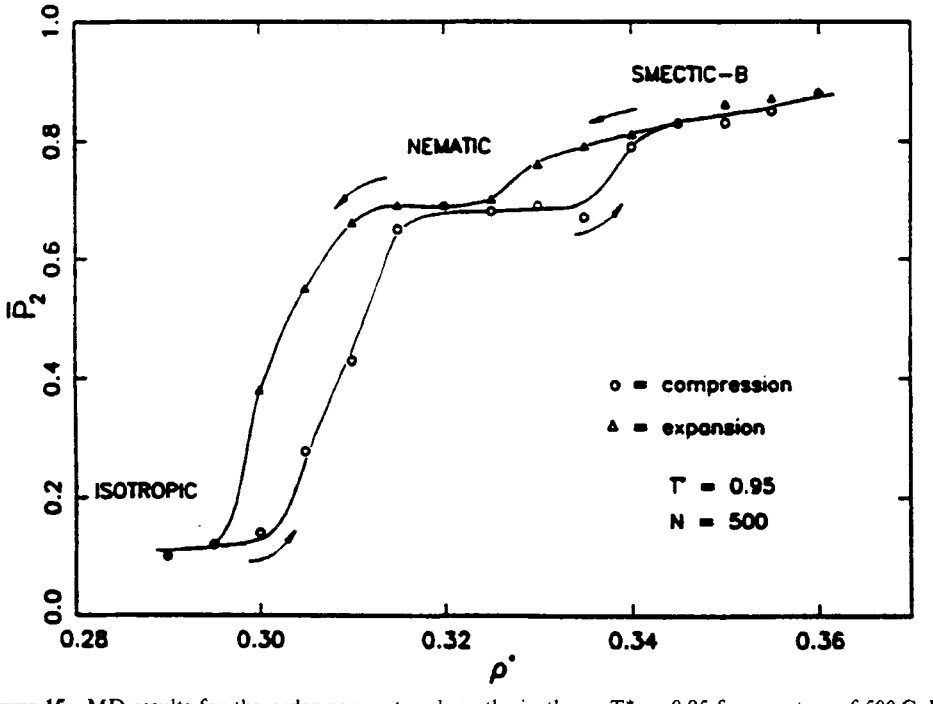

Figure 15 MD results for the order parameter along the isotherm $T^* = 0.95$ for a system of 500 G–B molecules. Circles are for the compression run, and triangles for the expansion run.

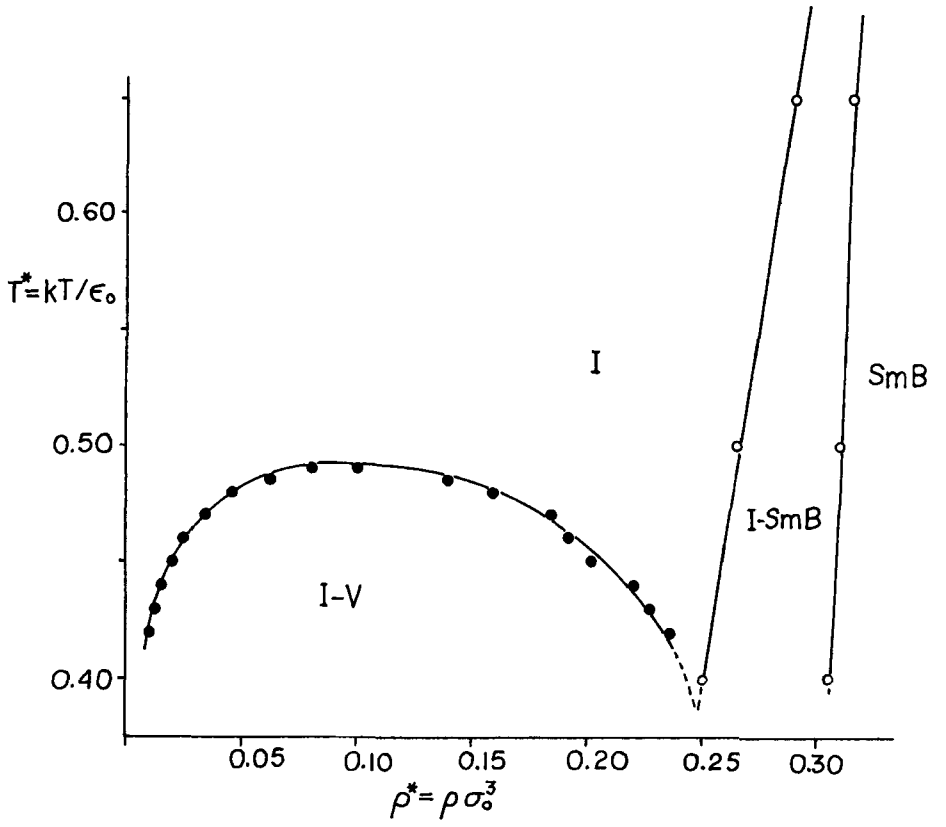

Figure 16 Approximate phase diagram for the G–B fluid with $\kappa = 3$, $\kappa' = 5$ for the low temperature region, based on Gibbs Ensemble Monte Carlo simulations (solid points) and approximate coexistence densities determined from MD isotherms (open circles) [11, 13]. The dashed lines serve as extrapolations from the given data. *V*, *I*, and *Sm*-B refer to vapour, isotropic liquid and smectic-B phases, respectively.

described here have suggested the presence of a transition from an orthogonal smectic-B to a tilt smectic-B phase. The location of this transition is also shown in Figure 17.

4 GAY–BERNE FLUID CONFINED IN A PORE

In this section we present preliminary results of *NVT* molecular dynamics simulations of a G–B fluid confined in a slit-like pore. The confinement effects of systems of mesogenic molecules have been studied theoretically using Landau–De Gennes type continuum models [20–22] and molecular models [16, 23–25]. The cases studied have mainly been for homeotropic wall-fluid interactions, i.e., walls that induce perpendicular alignment of the molecules near them. The homeotropic ordering allows a considerable simplification in the theory because the nematic is uniaxial, and in addition, breaks the translational symmetry of the bulk phase. These theories predict several qualitative effects of great interest, including: a first-order wetting

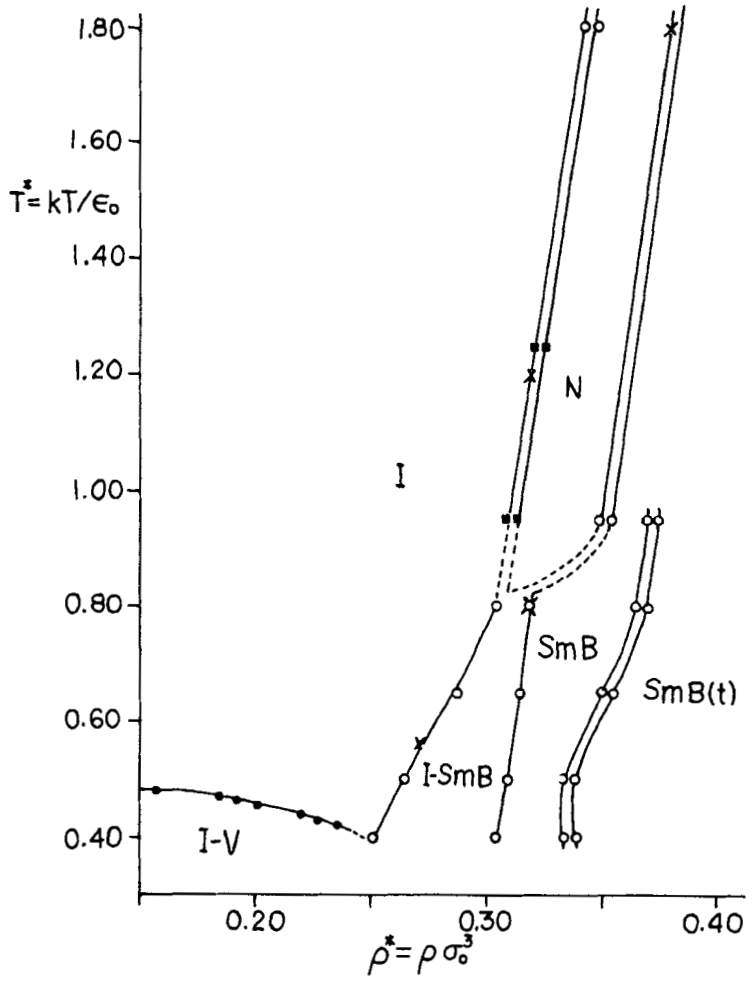

Figure 17 Approximate phase diagram for the high temperature region, showing vapour (*V*), isotropic liquid (*I*), nematic (*N*), smectic-B (*Sm*B), and tilt smectic-B (*Sm*B(*t*)) phases. Solid squares are nematic-isotropic liquid coexistence points determined from thermodynamic integration [2]; solid circles are from Gibbs Ensemble Monte Carlo calculations [13]; open circles are approximate results along isotherms using the methods described here [11, this work]; crosses are approximate results along isochores from this work.

transition (also called a boundary layer transition) at the wall at a temperature slightly above the bulk isotropic-nematic transition T_{IN}; shifts in T_{IN} to higher or lower temperatures; and the occurrence of an isotropic-nematic critical point (not present in the bulk fluid).

Previous simulations for systems of confined mesogens appear to have been limited to lattice models such as the Lebwohl–Lasher (L–L) model. Luckhurst and coworkers [26] have studied the surface properties of a thin liquid crystal film by MC simulations. They used a L–L system of 10 × 10 × 10 sites and applied periodic boundary conditions in just two dimensions, thus forming two free surfaces orthogonal to the

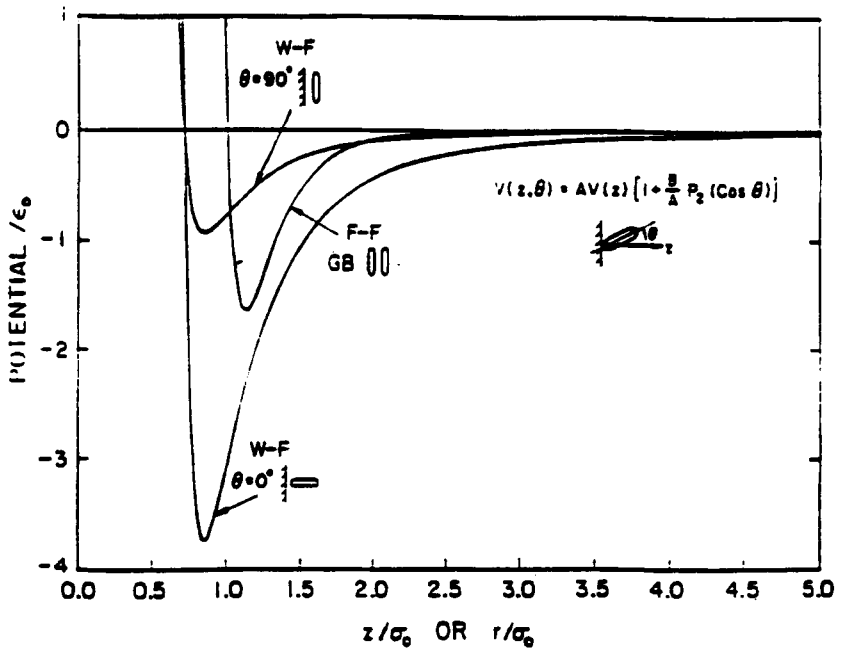

Figure 18 The wall-fluid potential for perpendicular and parallel orientations of the molecules with the wall, for $A = B = 1$ in Equation (1). The Gay–Berne fluid–fluid potential for molecules with their long axes parallel to one another is also shown for comparison.

third dimension. They found a very small downward shift in T_{IN} over the bulk value (due to the effect of free surfaces, and perhaps, a smaller system size), and also an isotropic phase adsorbed on the surface when there is a bulk nematic phase in the center of the pore. In his MC simulations, Allen [27] studied the same model as Luckhurst *et al.*, but at larger system sizes of $32 \times 32 \times L$ sites, where L, the thickness of the film, varies from 6–32. He observed a very small decrease in T_{IN} over the bulk value. A weak first order I–N transition persists in systems with $L \geqslant 8$ layers, but below this thickness the transition could not be detected. He thus tentatively concluded the existence of an I–N critical point at $L \approx 8$ layers. However, recent mean field calculations by Telo Da Gama and Tarazona [24] for the L–L model with free surfaces show that, contrary to the critical point suggested by the simulations, a first-order I–N transitions persists, even for two dimensional systems.

In this section we report initial results for the liquid crystal states of the confined Gay–Berne fluid. For the fluid confined between parallel walls two new variables are introduced, namely the wall separation H and the strength and nature of the fluid-wall interactions. Such simulations are complicated by long equilibration times and possible system size effects, so that the results reported here should be regarded as tentative. The conditions studied are shown in Table 4.

The fluid-wall potential, Equation (1), is shown in Figure 18 for the case of homeotropic alignment with $A = B = 1$ and $\rho\sigma_0^3 = 0.85$; the Gay–Berne fluid–fluid potential for the case of parallel molecules side-by-side is also shown for comparison. The well depth of the wall-fluid potential for a molecule oriented perpendicular to the

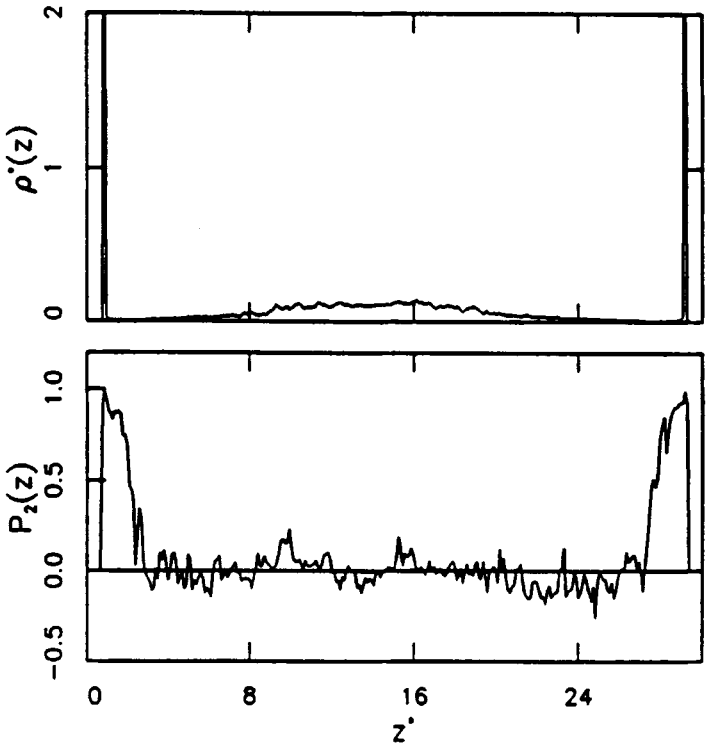

Figure 19 MD results for the density and order parameter profiles for 800 G–B molecules in a pore with $H^* = 30$, $(N/V)^* = 0.080$, and $T^* = 0.65$.

wall is much lower than the well depth of the fluid–fluid potential. For the isotherms the starting configuration was generated by cutting a slab of fluid of the required pore size from an f.c.c. lattice of 864 molecules at a density, $(N/V)^* = 0.02$. The system was subsequently compressed along the isotherm to higher densities, starting in all cases from the final configuration corresponding to the previous run. Since for any fluid in general, the effect of the pore is to lower the liquid-vapor critical point (see [28] for the case of a L–J fluid), and the corresponding bulk G–B fluid has a L–V critical point of $T_c^* = 0.49$, we expect the isotherms studied here ($T^* = 0.65$ and above) for the pore to lie in the supercritical region. The structure of the confined G-B fluid was studied by calculating the density and order parameter profiles in the pore. The system

Table 4 Details of the MD simulations for the confined fluid.

Run	*Type of Run*	*N*	*H**	*(N/V)**	*L**	*T**	ρ^*_{pore}	*Phases*
Isochore	Heating	256	14.7	0.41	6.5	1.0–3.5	0.32	*I, N, Sm*
Isochore	Cooling	256	14.7	0.41	6.5	1.0–3.5	0.32	*I, N, Sm*
Isotherm	Compression	800	30.0	0.08–0.36	8.6–18.3	0.65	0.06–0.34	*I, N, Sm*
Isotherm	Compression	800	30.0	0.08–0.36	8.6–18.3	0.95	0.06–0.34	*I*
Isotherm	Compression	800	30.0	0.08–0.36	8.6–18.3	1.25	0.06–0.34	*I*

[a] $L^* = L/\sigma_0$ where L is the length of the side of the wall, i.e. the dimension of the simulation box in the x or y direction.

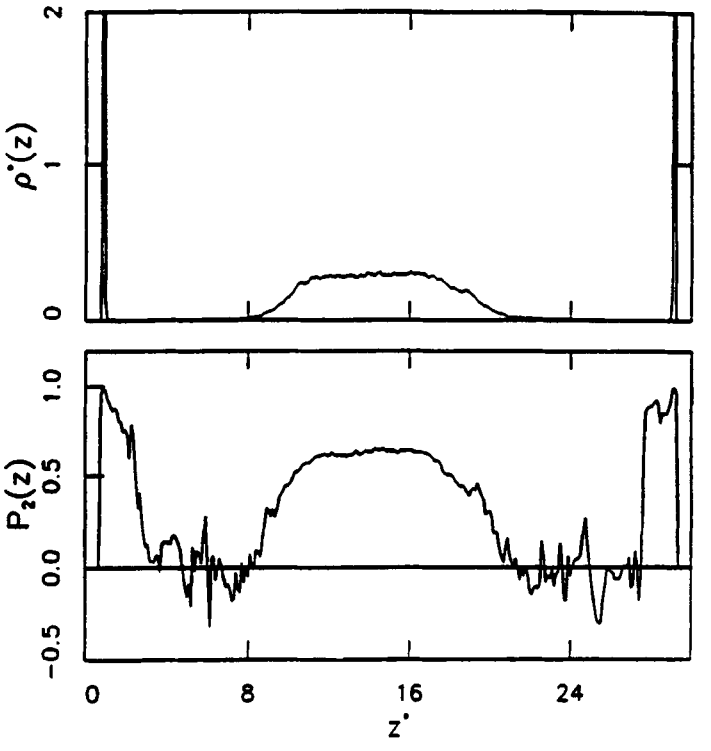

Figure 20 MD results for the density and order parameter profiles for 800 G–B molecules in a pore with $H^* = 30$, $(N/V)^* = 0.130$, and $T^* = 0.65$.

was completely equilibrated by checking the constancy of these profiles. In Figure 19 are shown results for $H^* = H/\sigma_0 = 30$ and $T^* = 0.65$ for the density profile, $\rho^*(z) = \rho(z)\sigma_0^3$, and the order parameter profile, $\bar{P}_2(z)$, when the overall density is $(N/V)^* = 0.08$; in this case, although there is homeotropic orientation near the wall, the liquid phase in the center of the pore is isotropic. The large peak in $\rho^*(z)$ indicates a solid-like monolayer adsorbed on the walls, with the molecules oriented perpendicular to them ($\bar{P}_2(z)$ is close to unity in this region). In the center of the cell $\bar{P}_2(z)$ oscillates about zero, indicating an isotropic phase there. Although the fluid shown in Figure 19 has an overall density of $(N/V)^* = 0.08$, the effective density in the center of the pore is only $\rho^*_{\text{pore}} = 0.06$, because of the solid-like monolayer adsorbed near the walls. On slowly compressing the system to the density $(N/V)^* = 0.130$, an orientational disorder–order transition takes place in the fluid in the center of the pore. The profiles at this density are shown in Figure 20, where in this case, $\rho^*_{\text{pore}} = 0.100$. The large positive values of $\bar{P}_2(z)$ in the center of the pore show that the fluid there is a nematic. The corresponding isotherm for the bulk fluid shows isotropic and smectic-B phases and an absence of any nematic phase. Thus we find that the pore stabilizes the occurrence of a nematic phase in the G–B fluid. On further compression, this nematic phase in the center of the pore persists until a density $(N/V)^* = 0.350$, where a layered structure of the fluid starts to appear. In Figure 21 are shown the profiles at a density $(N/V)^* = 0.36$; here $\rho^*_{\text{pore}} = 0.340$. The layered

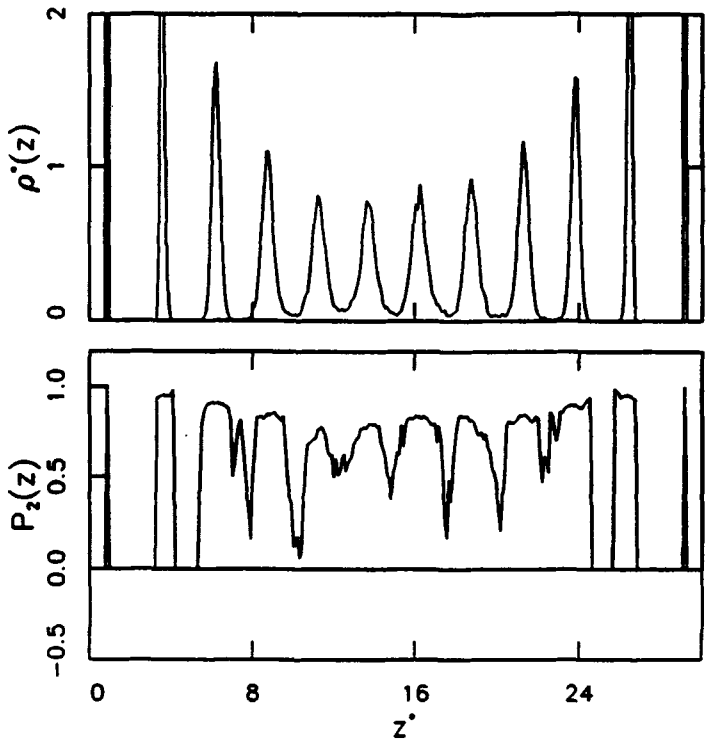

Figure 21 MD results for the density and order parameter profiles for 800 G–B molecules in a pore with $H^* = 30$, $(N/V)^* = 0.36$, and $T^* = 0.65$.

structure due to the walls (shown by the unequal peak-heights in $\rho^*(z)$ near the walls) persists up to a distance of $z = 10\sigma_0$ into the fluid. However, the fluid in the center of the pore shows equal peak-heights in the density profiles, thus indicating a smectic-like layered structure. The positions of the centers of masses of the molecules in each layer have a hexagonal arrangement (cf. the hexagonal arrangement for the bulk *Sm*B phase shown in Figure 7), so we identify the structure to be a hexagonal smectic-B phase. A summary of our results along the isotherm $T^* = 0.65$ for $H^* = 30$ is shown in Figure 22, together with the bulk fluid results for comparison. Here the average order parameter, η_{pore}, is the average of $\bar{P}_2(z)$ over a range of z that excludes molecules adjacent to the wall. The pore density for the isotropic-nematic transition seems to lie between 0.080 and 0.130. The nematic-smectic-B transition occurs for pore densities of 0.300 to 0.320; these latter values are approximately the same as those found for the isotropic-smectic-B transition for the bulk fluid (0.308 to 0.315).

Two other isotherms at higher temperatures ($T^* = 0.95$, 1.25) were also studied for a pore of $H^* = 30$. At these temperatures, compressing the isotropic phase does not appear to produce orientationally ordered phases, even at high densities. The reason may be that the system is trapped in a metastable state, and the higher kinetic energy of the molecules inhibits the formation of orientationally or translationally ordered phases. A similar situation was observed for the bulk fluid at $T^* = 1.25$ and 1.8, where compressing the nematic phase did not result in the formation of layered phases.

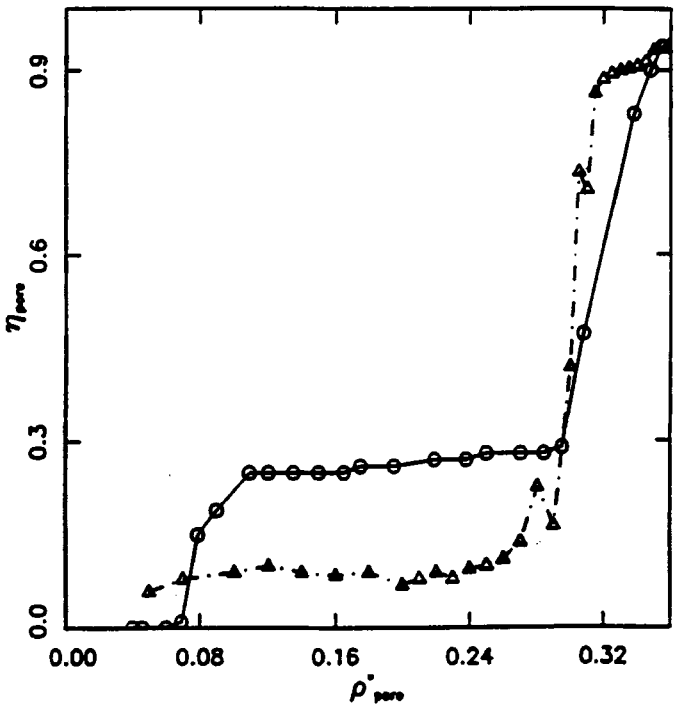

Figure 22 MD results for the order parameter for 800 G–B molecules in a pore with $H^* = 30$ along the isotherm $T^* = 0.65$. The abscissa ρ^*_{pore} is the density in the center of the pore. Circles represent results for a pore of size $H^* = 30$; triangles are for the bulk fluid ($H^* = \infty$). Lines are drawn through the points as a guide to the eye.

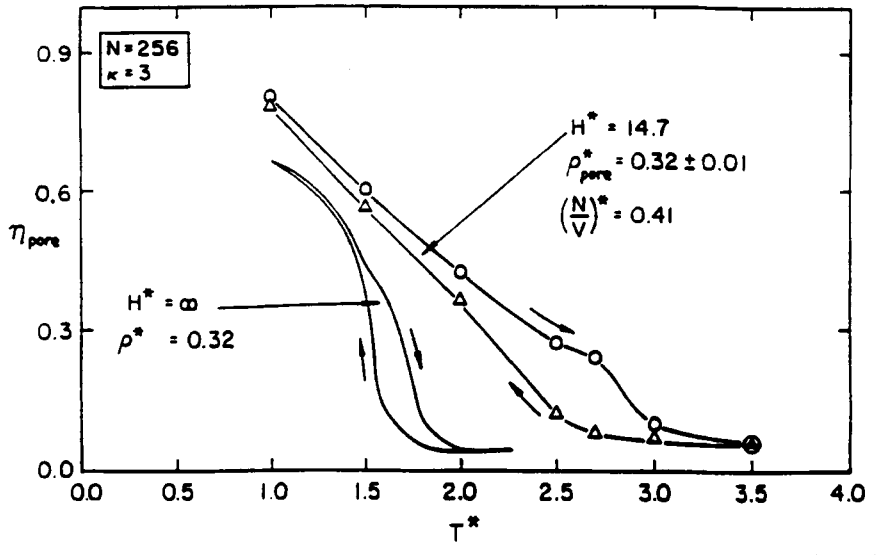

Figure 23 The average order parameter, η_{pore}, for 256 G–B molecules in a pore with $H^* = 14.7$, $(N/V)^* = 0.41$; the density in the centre of the pores is $\rho^*_{pore} = 0.32$. The results for the bulk fluid ($H^* = \infty$) at the same density are shown for comparison.

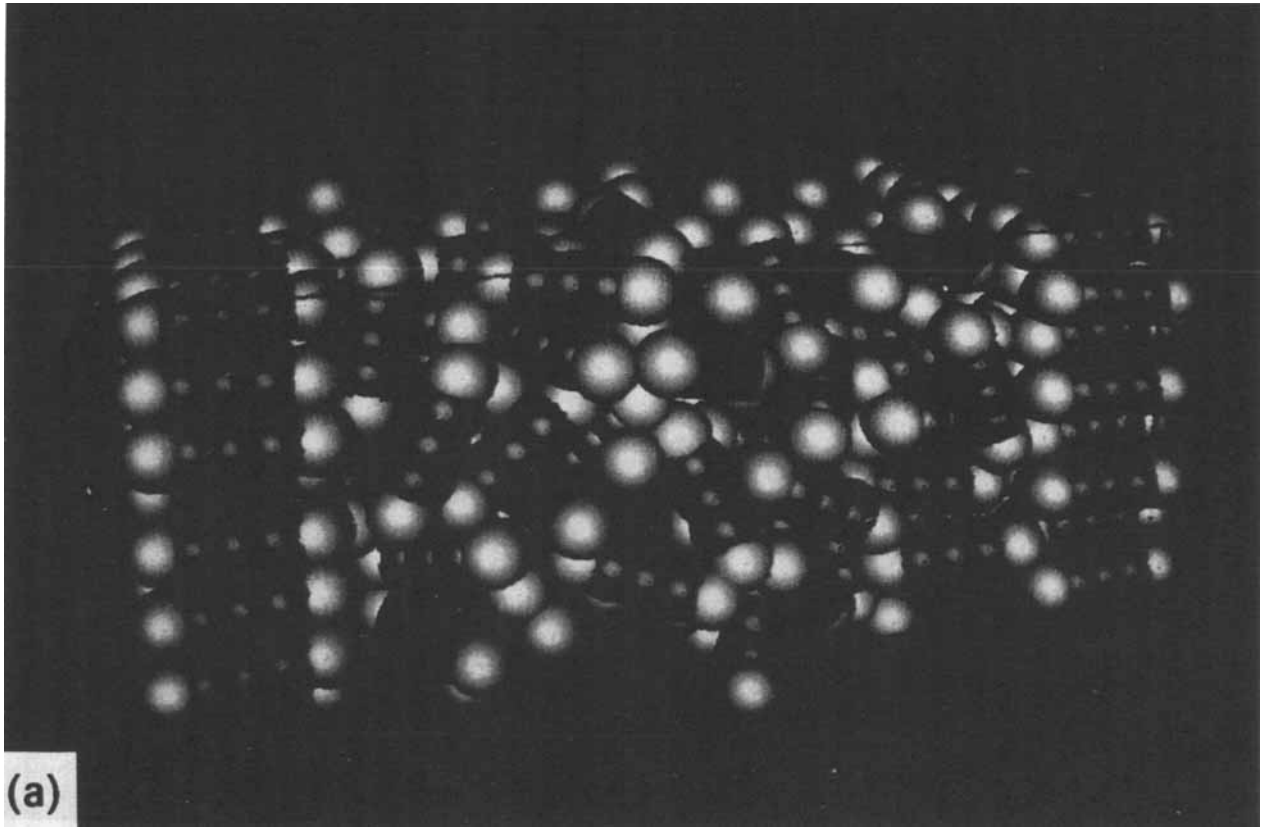

Figure 24 Snapshots of the final configurations for MD simulations for a pore of $H^* = 14.7$. The G–B molecule is represented as a spherocylinder made up of 5 overlapping spheres; the middle 3 spheres are coloured green and the end spheres red. In (a) $(N/V)^* = 0.32$, $T^* = 1.8$, yielding an isotropic phase in the pore centre; (b) $(N/V)^* = 0.41$, $T^* = 1.0$, with the sizes of the molecules reduced to 25% of normal size, yielding a nematic phase (See color plates VI and VII).

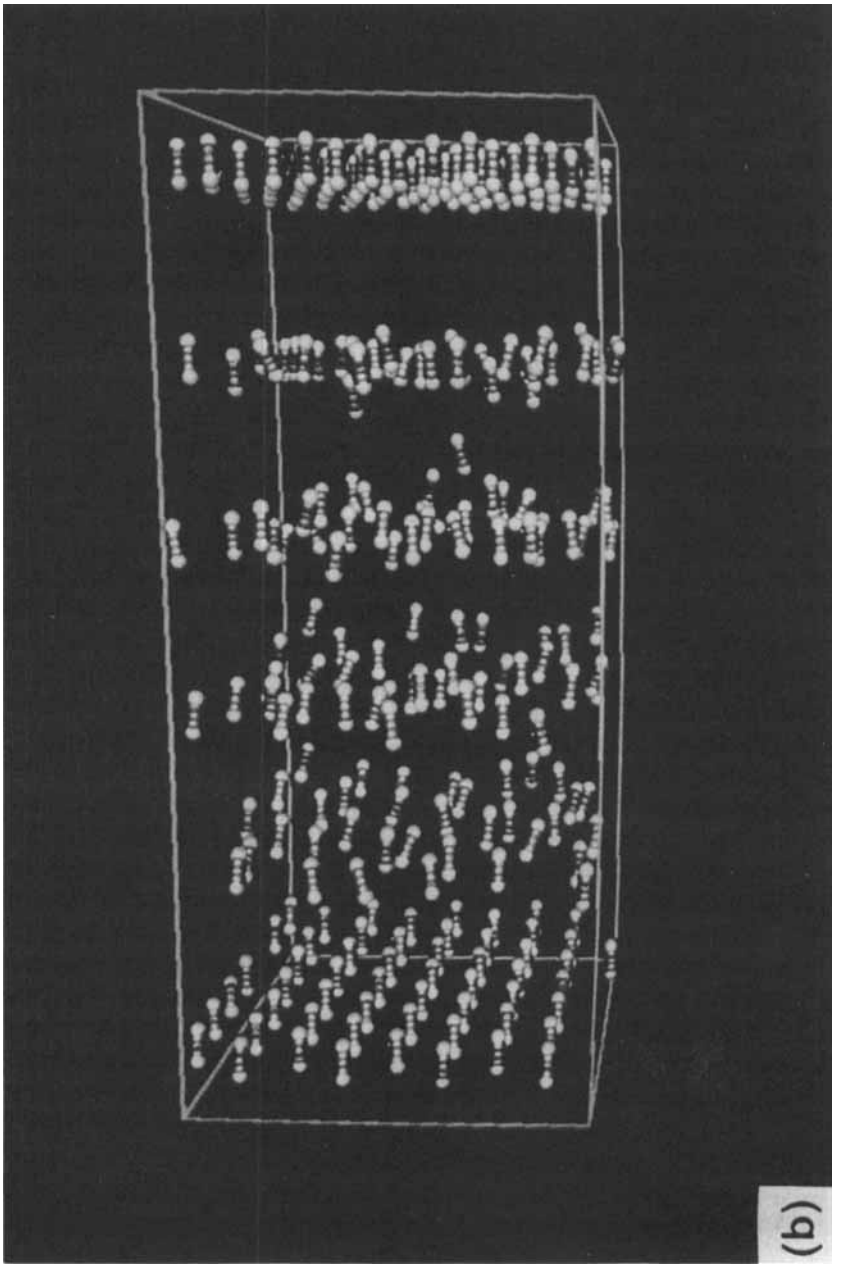

Figure 24 (*Continued*)

Simulations along the isochore $(N/V)^* = 0.41$ have also been carried out for 256 molecules in a pore of width $H^* = 14.7$, using both heating and cooling runs. The density in the pore centre, after excluding the molecules in the solid-like layers near each wall, is $\rho^*_{\text{pore}} \approx 0.32$. At $T^* = 1.0$, for example, the values of $\bar{P}_2(z)$ in the centre of the cell are found to be a little below unity, indicating an orientationally ordered phase. The density profile near the pore centre shows smectic-like layering of the fluid. No such orientational ordering or layering occurs in the bulk fluid at $T^* = 1.0$ and $\rho^* = 0.32$, so that the confinement between homeotropic walls again stabilizes the liquid crystal phase. Although the density profile at $T^* = 1.0$ in the pore shows layering, and snapshots of the structure in the xy plane show a hexagonal arrangement in each layer, the unequal peak heights for $\rho(z)$ near the pore center suggest that the layering is a consequence of the confinement of the fluid by the pore walls. A summary of our results for $H^* = 14.7$ is shown in Figure 23, where the average order parameter, η_{pore}, is shown for both the bulk fluid and the fluid in the pore. Although there are strong hysteresis effects, the NI transition temperature seems to lie between 2.5 and 3.0, significantly above the bulk fluid value (about 1.7). Thus, these results confirm that the wall forces tend to stabilize the nematic phase. Snapshots of typical configurations are shown in Figure 24 for temperatures in the isotropic liquid and in the nematic regions, respectively.

5 CONCLUSIONS

Using Gibbs ensemble and MD techniques, we have constructed an approximate phase diagram for the bulk G-B fluid with $\kappa = 3$, $\kappa' = 5$. The system is found to exhibit a series of phases as the temperature is lowered or the density is increased. These phases have been identified from plots of the fluid structure and snapshots of the molecular configurations to be the vapor, isotropic liquid, nematic and smectic-B phase. We find evidence of a vapor-isotropic-smectic-B and an isotropic-nematic-smectic-B triple point.

For homeotropic pores, the confined G–B fluid exhibits an isotropic-nematic transition that is similar in nature to that of the bulk transition; however the pore fluid exhibits a nematic phase at state conditions where no such phase occurs in the corresponding bulk fluid. Thus the confined G–B fluid stabilizes the nematic phase at conditions below the *I-N-Sm*B triple point in the bulk G–B fluid. The pore also appears to induce smectic phases at slightly higher densities than those observed for the bulk fluid.

This rich phase behavior of the Gay–Berne model fluid makes it a useful system with which to enhance our understanding of the static and dynamic properties of real liquid crystals.

Acknowledgements

We are grateful to the National Science Foundation (grant no. CTS-8914907) and to NATO for support of this work.

References

[1] D.J. Adams, G.R. Luckhurst and R.W. Phippen, "Computer simulation studies of anisotropic systems XVII. The Gay–Berne model nematogen", *Mol. Phys.*, **61**, 1575 (1987).

[2] E. de Miguel, L.F. Rull, M.K. Chalam, K.E. Gubbins and F. van Swol, "Location of the isotropic-nematic transition in the Gay–Berne model", *Mol. Phys.*, **72**, 593 (1991).
[3] B. Tjipto-Margo and D.E. Sullivan, "Molecular interactions and interface properties of nematic liquid crystals", *J. Phys. Chem.*, **88**, 6620 (1988).
[4] D. Frenkel, H.N.W. Lekkerkerker and A. Stroobants, "Thermodynamic stability of a smectic phase in a system of hard rods", *Nature*, **332**, 822 (1988).
[5] D. Frenkel, "Columnar ordering as an excluded-volume effect", *Liq. Cryst.*, **5**(3), 929 (1989).
[6] D. Frenkel, "Structure of hard-core models for liquid crystals", *J. Phys. Chem.*, **92**, 3280 (1988).
[7] D. Frenkel, "Computer simulation of hard-core models for liquid crystals", *Mol. Phys.*, **60**, 1 (1987).
[8] R. Eppenga and D. Frenkel, "Monte Carlo study of the isotropic and nematic phases of infinitely thin hard platelets", *Mol. Phys.*, **52**, 1303 (1984).
[9] D. Frenkel and B.M. Mulder, "The hard ellipsoid-of-revolution fluid I. Monte Carlo simulations", *Mol. Phys.* **55**, 1171 (1985).
[10] M.P. Allen and D. Frenkel, "Observation of dynamical precursors of the isotropic-nematic transition by computer simulation", *Phys. Rev. Lett.*, **58**, 1748 (1987).
[11] E. de Miguel, L.F. Rull, M.K. Chalam and K.E. Gubbins, "Liquid crystal phase diagram of the Gay–Berne fluid", *Mol. Phys.*, in press (1991).
[12] G.R. Luckhurst, R.A. Stephens and R.W. Phippen, "Computer simulation studies of anisotropic systems XIX. Mesophases formed by the Gay–Berne model nematogen", *Liquid Crystals*, in press (1991).
[13] E. de Miguel, L.F. Rull, M.K. Chalam and K.E. Gubbins, "Liquid–vapour coexistence of the Gay–Berne fluid by Gibbs ensemble simulation", *Mol. Phys.*, **71**, 1123 (1990).
[14] A.Z. Panagiotopoulos, "Direct determination of phase coexistence properties of fluids by Monte Carlo simulation in a new ensemble", *Mol. Phys.*, **61**, 813 (1987); "Adsorption and capillary condensation of fluids in cylindrical pores by Monte Carlo simulation in the Gibbs ensemble", *Mol. Phys.*, **62**, 701 (1987).
[15] C. Zannoni, "Distribution functions and order parameters", in *The Molecular Physics of Liquid Crystals*, G.R. Luckhurst and G.W. Gray, eds, Academic, Press, London, 1979, ch. 9.
[16] M.M. Telo da Gama, "The interfacial properties of a model of a nematic liquid crystal I. The nematic-isotropic and the nematic-vapour interfaces", *Mol. Phys.*, **52**, 585 (1984); "The interfacial properties of a model of a nematic liquid crystal II. Induced orientational order and wetting transitions at a solid-fluid interface", *Mol. Phys*, **52**, 611 (1984).
[17] W.A. Steele and G.D. Hasley, "The interaction of gas molecules with capillary and crystal lattice surfaces", *J. Phys. Chem.*, **59**, 57 (1955).
[18] P.S. Pershan, "Structure of liquid crystal phases", in *World Scientific Lecture Notes in Physics*, vol. 23, World Scientific, New Jersey, (1988).
[19] M.P. Allen and D.J. Tildesley, *Computer Simulations of Liquids*, Clarendon Press, Oxford, (1987).
[20] P.G. de Gennes, *The Physics of Liquid Crystals*, Clarendon Press, Oxford, (1974).
[21] P. Sheng, "Boundary-layer phase transition in nematic liquid crystals", *Phys. Rev. A*, **26**, 1610, (1982).
[22] A. Poniewierski and T.J. Sluckin, "Theory of the nematic-isotropic transition on a restricted geometry" *Liq. Cryst.*, **2**, 281, (1987); see also T.J. Sluckin and A. Poniewierski, "Orientational wetting transitions and related phenomena in nematics", in *Fluid Interfacial Phenomena*, C.A. Croxton, ed, Wiley, 1986, ch. 5.
[23] H. Schroder, "Molecular statistical theory for inhomogeneous nematic liquid crystals with boundary conditions", *J. Chem. Phys.*, **67**(1), 16 (1977).
[24] M.M. Telo da Gama and P. Tarazona, "First-order and continuous transitions in confined liquid crystals", *Phys. Rev. A*, **41**, 1149 (1990).
[25] M.M Telo da Gama, P. Tarazona, M.P. Allen and R. Evans, "The effect of confinement on the isotropic-nematic transition", *Mol. Phys.*, **71**, 801 (1990).
[26] G.R. Luckhurst, T.J. Sluckin and H.B. Zewdie, "Computer simulation studies of anisotropic systems XV. The surface properties of the Lebwohl-Lasher model nematogen", *Mol. Phys.*, **59**, 657 (1986).
[27] M.P. Allen, "Computer simulation of liquid crystal films", *Mol. Sim.*, **4**, 61 (1989).
[28] B.K. Peterson, K.E. Gubbins, G.S. Heffelfinger, U. Marini Bettolo Marconi and F. van Swol, "Lennard–Jones fluids in cylindrical pores: Nonlocal theory and computer simulation", *J. Chem. Phys.*, **88**, 6487 (1988).